Front. For. China 2009, 4(4): 402–408
DOI 10.1007/s11461-009-0057-8

RESEARCH ARTICLE

Zhujun GU, Zhiyuan ZENG, Xuezheng SHI, Dongsheng YU, Wei ZHENG, Zhenlong ZHANG, Zifu HU

Estimating models of vegetation fractional coverage based on remote sensing images at different radiometric correction levels

Abstract The images of post atmospheric correction reflectance (PAC), top of atmosphere reflectance (TOA), and digital number (DN) of a SPOT5 HRG remote sensing image of Nanjing, China were used to derive four vegetation indices (VIs), that is, normalized difference vegetation index (NDVI), transformed vegetation index (TVI), soil-adjusted vegetation index (SAVI), and modified soil-adjusted vegetation index (MSAVI). Based on these VIs and the vegetation fractional coverage (VFC) data obtained from field measurements, thirty-six VI-VFC relationship models were established. The results showed that cubic polynomial models based on NDVI and TVI from PAC were the best, followed by those based on SAVI and MSAVI from DN, with their accuracies being slightly higher than those of the former two models when VFC > 0.8. The accuracies of these four models were higher in medium densely vegetated areas (VFC = 0.4 – 0.8) than in sparsely vegetated areas (VFC = 0 – 0.4). All the models could be used elsewhere via the introduction of a calibration model. In VI-VFC modeling, using VIs derived from different radiometric correction levels of remote sensing images could help explore and show valuable information from remote sensing data and thus improve the accuracy of VFC estimation.

Keywords radiometric correction, vegetation index, vegetation fractional coverage, model

Translated from *Chinese Journal of Applied Ecology*, 2008, 19(6): 1296–1302 [译自: 应用生态学报]

Zhujun GU
School of Geography Science, Nanjing Xiaozhuang University, Nanjing 211171, China

Zhujun GU, Xuezheng SHI, Dongsheng YU
State Key Laboratory of Soil and Sustainable Agriculture, Institute of Soil Science, Chinese Academy of Sciences, Nanjing 210008, China

Zhujun GU, Zhiyuan ZENG (✉), Wei ZHENG, Zhenlong ZHANG, Zifu HU
School of Geography Science, Nanjing Normal University, Nanjing 210097, China
E-mail: zhujungu@163.com

Zhujun GU, Xuezheng SHI
Graduate University of Chinese Academy of Sciences, Beijing 100039, China

1 Introduction

Vegetation fractional coverage (VFC) is a key parameter in studies of landscape ecology (Zhao et al., 2004; Chen et al., 2006; Gong and Xia, 2006), climate change (Sun et al., 2001; Lin and Qi, 2004), and soil erosion (Gao et al., 2001, Hai et al., 2002; He et al., 2005). Since the 1970s, VFC monitoring via remote sensing has been developed vigorously. During this period, we have always been concerned with the question on how to tap remote sensing information in useful ways and to improve the efficiency and accuracy of VFC estimations. Among many methods, a relationship model based on regression analysis of remote sensing data and VFC is both simple and convenient, and it has now been widely accepted. A large number of investigators reported various relationships between VFC and remote sensing information from different bands or band combinations of images (Graetz et al., 1988; North, 2002; Liu et al., 2006a; Zhang et al., 2007) and thought that vegetation indices play important roles in VFC estimation. Among these vegetation indices, the normalized difference vegetation index (NDVI) has been most widely used (Dymond et al., 1992; Wittich and Hansing, 1995). However, the larger the amount of vegetation, the stronger the "saturation effect" of NDVI appears (i.e., sensibility of NDVI to VFC changes decreases (Carlson et al., 1990)). Moreover, NDVI is affected by soil background, which will also lead to errors in VFC estimation (Huete and Jackson, 1988). Consequently, more vegetation indices should be used in VFC estimation (Eastwood et al., 1997; Gitelson et al., 2002).

Both the single band and the vegetation index of remote

sensing images are affected by image noise, which is caused by sensor decay over time or by atmospheric reflection and absorption of electromagnetic energy, so radiometric correction is part of the technology of quantitative remote sensing. Accurate radiometric correction includes many aspects such as radiometric calibration, atmospheric correction, relief correction, and sometimes sun glint effect and the comprehensive effect of nearby pixels. All of these factors make radiometric correction a challenging task with uncertain accuracies (Abdou et al., 2000). Some studies indicate that radiometric correction does improve the accuracy of the inversion of vegetation parameters (Liang et al., 2002; Liu et al., 2006b), whereas others insist that no remarkable effect of radiometric correction appears (Qi et al., 2000). Therefore, in quantitative remote sensing of vegetation parameters, the impact of radiometric correction on the estimation of vegetation parameters involves uncertainties and needs to be investigated further.

Although there are many reports of VFC estimation in the literatures, most are aimed at a specific kind of vegetation, whereas few are concerned with the effect of radiometric correction or with methods of how to use models elsewhere. In view of these concerns, various VFC estimation models were established in this paper, based on different radiometric correction levels of SPOT images for areas with different types of vegetation. The use of models in other areas is also recommended, to give technical support for VFC estimation in a wider basis.

2 Materials and methods

2.1 Study site

Our study site was located in urban and suburban districts of Nanjing, China (31°56′–32°1′N, 118°38′–118°53′E), with a total area of about 790 km^2. The topography of the area consists of low mountains, hills, and plains along the Yangtze River. At 448 m, Purple Mountain is the highest point, found southeast of the urban center. A northern subtropical monsoon climate prevails in the area, with a mean annual temperature of 15.1°C and mean annual precipitation of 1019 mm. The main vegetation types are trees, shrubs, and grasses. The grasses are mainly distributed over the plains alongside the Yangtze River, whereas shrubs and trees are largely found in the hilly areas with gentle slopes of less than 20°.

2.2 Methods

2.2.1 Data sources

One remote sensing image, 1A grade level, acquired on November 9, 2002, from SPOT5 HRG sensor (SN: 290, LN: 286; SPOT Image Co., Beijing, China) was used. Only infrared and red bands of the image, both with 10-m spatial resolution, were selected for further analyses. Besides, a 1∶10000 relief map, a 1∶50000 land use map, and a map of vegetation types with a scale of 1∶600,000 were used as the data basis to aid the selection and layout of field measurements (Jiangsu Bureau of Surveying and Mapping, 1997).

2.2.2 VFC field measurements

Aided by relief and vegetation maps, 23 sampling sites were selected according to access, perceived representation, and being relatively undisturbed (Ringrose et al., 2003). The vegetation types include forests where ten sample sites were established, shrubs with four sites, and grasslands with six sample sites, as well as three nonvegetation sites (two bare land sites and one water surface). Then, 129 quadrats, with 10 × 10 m dimensions each (the same as that of the spatial resolution of the SPOT image) were arranged, plotting 3–8 quadrats in each site (Fig. 1). The position of each quadrat was determined using a GPS of Starlink Invicta210 (RAVEN Industries, NC, USA). In addition, the locations of 23 ground control points (GCP), including road intersections and middle parts of bridges, were logged for image geometric correction.

VFC measurements were conducted in November 2004 using a vertical photography method (Zhang et al., 2001; Gemmell et al., 2001), with a digital camera with spatial resolution of 2592 × 1944. The objects in each photo were classified into vegetation and nonvegetation types via the remote sensing image processing software ENVI version 4.0. The percentage of vegetation pixels on each photo (i.e., VFC) was calculated and reported automatically (Purevdorj et al., 1998). Quadrats of VFC were acquired by averaging VFCs from all photos taken on each quadrat.

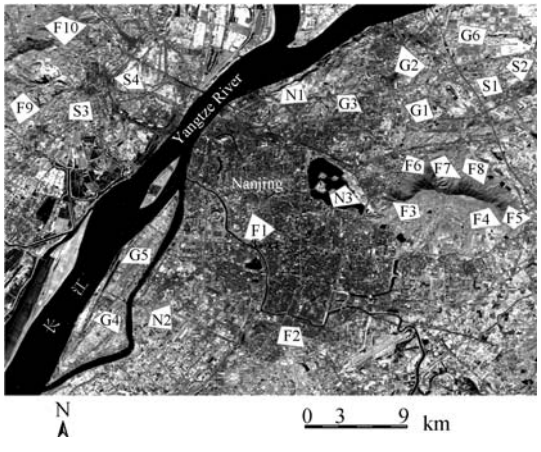

Fig. 1 Location of the sample site. F: forest site; S: shrub site; G: grassland site; N: nonvegetation site.

2.2.3 Image preprocessing and extraction of vegetation indices

To normalize the coordinate system, a geometric correction was carried out for the SPOT5 image, using a quadratic polynomial model with the 23 GCPs and resampled via a nearest neighbor algorithm. The root mean squared error (RMSE) of the geometric correction was less than 1 pixel.

The radiometric correction was conducted as follows:

First, radiometric calibration was carried out to calculate spectral radiance at the top of the atmosphere (L^i_{sat}) ($(\text{m}^2\cdot\text{sr}\cdot\mu\text{m})/\text{W}$):

$$L^i_{\text{sat}} = \frac{\text{DN}_i}{G_i} \tag{1}$$

where i is the image band number, DN_i is the digital number of the ith band, and G_i is the calibration coefficient of the ith band ($(\text{m}^2\cdot\text{sr}\cdot\mu\text{m})/\text{W}$).

Next, the reflectance at the top of the atmosphere (i.e., the apparent reflectance (R^i_{sat})) was calculated:

$$R^i_{\text{sat}} = \frac{d^2\pi L^i_{\text{sat}}}{E^i_0\cos\theta} \tag{2}$$

where d is the normalized sun–earth distance at the time the image was acquired, E^i_0 is the exo-atmospheric radiation entering the atmosphere, and θ is the sun zenith angle.

Finally, the surface reflectance of ground objects (ρ_i) was acquired after atmospheric correction with a dark-object method (Song et al., 2001) using the following relationship:

$$\rho_i = \frac{d^2\pi(L^i_{\text{sat}} - L^i_{\text{p}})}{T^i_{\text{v}}(T^i_{\text{z}}E^i_0\cos\theta + E^i_{\text{down}})} \tag{3}$$

where T_{v} and T_{z} are the transmittance of the atmosphere in the view and illumination directions, respectively, E^i_{down} is the downwelling diffuse radiation and is set at 0 because this method assumes that there is no diffuse downwelling radiation (Chavez, 1988), and L^i_{p} is the path radiance due to atmospheric effects. L^i_{sat} and L^i_{p} are obtained by converting the minimum digital number in each band i into radiance (Soudani et al., 2006):

$$L^i_{\text{p}} = L^i_{\text{sat-min}} - \frac{0.01(T^i_{\text{z}}E^i_0\cos\theta + E^i_{\text{down}})T^i_{\text{v}}}{d^2\pi} \tag{4}$$

where $L^i_{\text{sat-min}}$ is the radiance corresponding to the minimum DN value from which there is a sharp increase in the number of pixels (Soudani et al., 2006).

Subsequently, images at three radiometric correction levels were acquired, that is, post atmospheric correction reflectance (PAC), top of atmosphere reflectance (TOA), and digital number (DN). Four kinds of vegetation indices (VI), including NDVI, transformed vegetation index (TVI), soil-adjusted vegetation index (SAVI), and modified soil-adjusted vegetation index (MSAVI) (Table 1) were derived from images at PAC, TOA, and DN levels, respectively, yielding 12 VI images, where VI values of 129 quadrats were extracted. To reduce the location errors, a quadrat-centered 20-m-long square buffer was made for each quadrat during the VI derivation.

2.2.4 VI-VFC modeling

To develop models to estimate VFC, the data from 129 quadrats were first separated into two independent subsets for model establishment (M) and validation (V). Subsets of 86 quadrats from M and 43 quadrats from V were selected in an M-V-M cycling sequence after sorting VFC values of all 129 quadrats in ascending order. Finally, linear, quadratic, and cubic polynomial models of the 12 VI-VFC combinations were established, yielding 36 models. The accuracy of each model was validated by R^2 and root mean squared error (RMSE) analysis using the following relationship:

$$\text{RMSE} = \left[\sum_{i=1}^{N}(e_i)^2/N\right]^{1/2} \tag{5}$$

where N represents the number of validation quadrats (43) and e_i is the estimation error (i.e., the difference between the measured VFC and the estimated VFC of quadrat i).

2.3 Data processing

Correlation analyses and VI-VFC modeling were performed using SPSS, version 13.0 (SPSS Inc., USA).

Table 1 Spectral vegetation indices NDVI, TVI, SAVI, and MSAVI

vegetation index	formula	reference
NDVI	$\text{NDVI} = \frac{\text{NIR}-R}{\text{NIR}+R}$	Rouse et al. (1973)
TVI	$\text{TVI} = \sqrt{\frac{\text{NIR}-R}{\text{NIR}+R}+0.05}$	McDaniel and Haas (1982)
SAVI	$\text{SAVI} = (1+L)\frac{\text{NIR}-R}{\text{NIR}+R+L}$	Huete and Jackson (1988)
MSAVI	$\text{MSAVI} = \text{NIR}+0.5-0.5\sqrt{(2\text{NIR}+1)^2-8(\text{NIR}-R)}$	Qi et al. (1994)

Note: NIR and R are near-infrared and red values, respectively. L is a canopy background adjustment factor, set at 0.5.

3 Results and analyses

3.1 VI-VFC relationship models

As shown in Fig. 2, on different VFC ranges of all vegetation types, positive relationships exist between VFC values and VIs derived from PAC, and the relationships at other radiometric correction levels are similar to those at PAC and are not shown in this paper. R^2 of the 36 VI-VFC models ranged between 0.37 and 0.73, and RMSE ranged from 0.14 to 0.16, indicating large differences in the reliability of all models. To compare such differences more clearly, R^2 histograms of the 36 models were plotted (Fig. 3), from which we can see the R^2 values of the models based on 3 radiometric correction levels ranked as PAC > DN > TOA, whereas at all radiometric correction levels, R^2 values of the polynomial models show linear ⩽ quadratic ⩽ cubic. R^2 differences of the models are dependent on vegetation indices and radiometric correction levels.

Among the models, cubic polynomial models based on NDVI and TVI from PAC are the best, followed by those based on SAVI and MSAVI from DN (Fig. 3 and Table 2). Therefore, these four models were selected for further analyses.

3.2 Model accuracy on different VFC ranges

On different VFC ranges, the accuracy of the four selected models can vary considerably. RMSEs are largest when VFC = 0 – 0.4, followed by conditions where VFC > 0.8 and VFC = 0.4 – 0.8. This presents that model accuracies in medium densely vegetated areas, where VFC = 0.4 – 0.8, are higher than those in sparsely vegetated areas where VFC = 0 – 0.4, showing the impact of soil background on spectral signals of surface objects (Carlson et al., 1990;

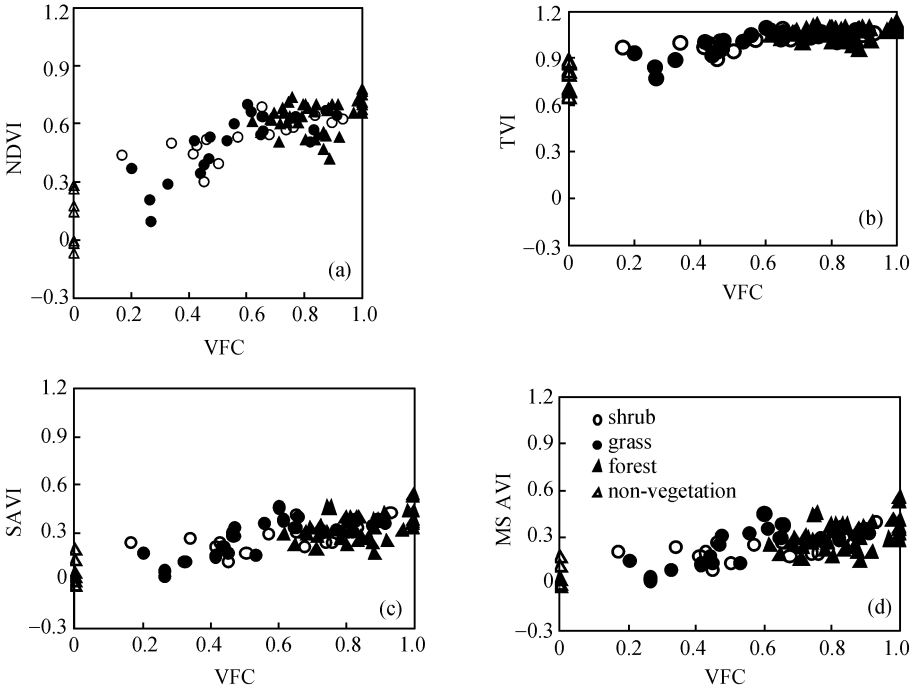

Fig. 2 Relationships between VFC and vegetation indices (VI) derived from post atmospheric correction reflectance of SPOT 5 imagery.

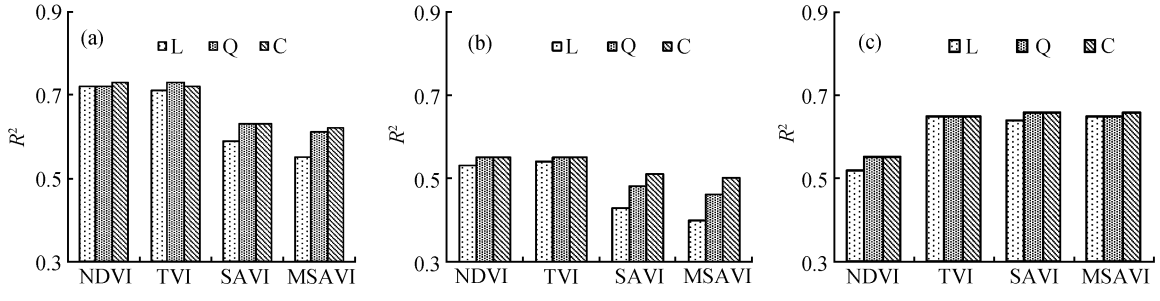

Fig. 3 R^2 of the VI-VFC relationship models based on three image processing levels. a: PAC; b: TOA; c: DN.
Note: L, Q, and C refer to linear, quadratic, and cubic polynomial models, respectively.

Table 2 Selected regressions between VI and VFC ($VFC = cons + b_1VI + b_2VI^2 + b_3VI^3$)

vegetation index	regression coefficients				R^2	RMSE
	cons	b_1	b_2	b_3		
NDVI[a]	0.005	0.097	3.689	−2.966	0.734	0.141
TVI[a]	−0.391	0.000	0.212	0.769	0.724	0.144
SAVI[b]	0.663	0.941	−0.635	−0.422	0.658	0.164
MSAVI[b]	0.669	0.685	−0.155	−0.229	0.655	0.162

Note: [a] Vegetation indices derived from reflectance of SPOT 5 image, after atmospheric correction; [b] Vegetation indices derived from digital number of SPOT 5 image. The same comments apply to Table 3 below.

Huete and Jackson, 1988). These results are different from those of studies on the grasslands of Inner Mongolia and Japan by Purevdorj et al. (1998), who reported that accuracies of VI-VFC models in sparsely vegetated areas (VFC < 0.4) are higher than those in medium and densely vegetated areas (VFC > 0.4). These differences may be related to the different geographic surroundings and sample characteristics. The quadrats of our study prevail on medium densely vegetated areas (Fig. 2), whereas the grasslands of Inner Mongolia and Japan measured by Purevdorj et al. (1998) were mainly sparsely vegetated.

Our four selected models are based on PAC and DN radiometric correction levels. From our analyses of the accuracy of the models based on these two correction levels, we can see that when VFC > 0.8, the accuracies of the cubic polynomial models based on SAVI and MSAVI from DN are slightly higher than those based on NDVI and TVI from PAC (Fig. 4). This indicates that under certain radiometric correction levels, SAVI and MSAVI have a stronger capability of "antisaturation" effect (Gitelson et al., 2002). The mechanism of such antisaturation needs further analysis. In VI-VFC modeling, using vegetation indices derived from different radiometric correction levels is helpful for mining information from remote sensing images and improving the accuracy of VFC estimation. In addition, integrating the vegetation indices with other remote sensing information and modeling through other statistical algorithms are also worthwhile for further investigations (Cai et al., 2005).

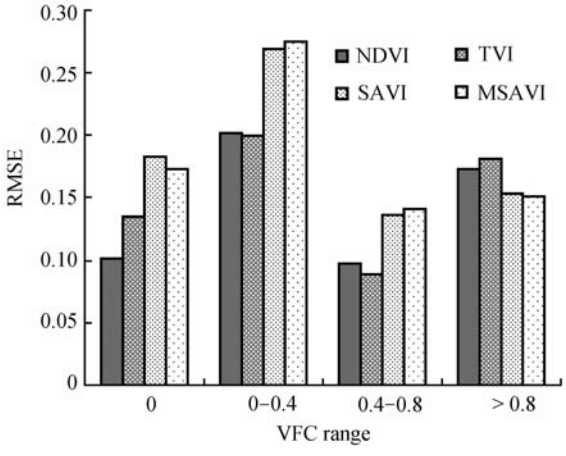

Fig. 4 RMSE of models on different VFC ranges
Note: Each vegetation index means a corresponding cubic polynomial model, where NDVI and TVI were derived from reflectance data after atmospheric correction and SAVI and MSAVI from digital numbers.

3.3 Model applications

VI-VFC models established in this paper are based on the entire image, so they can be used for VFC estimation on the entire study areas. For nonvegetated areas where VFC = 0, surface objects such as rivers, buildings, and typical bare lands should be erased with a mask tool after a classification procedure in the ENVI software. Then nonvegetated areas are not involved in VFC estimation, which will help improve the accuracy of VFC mapping. However, the classification of vegetation and nonvegetation needs further refinement (Yu et al., 2006). Fig. 5(a) and 5(b) are the resulting images of VFC calculation based on NDVI from PAC and MSAVI from DN, respectively. The contrasts in Fig. 5(a) are better than those in Fig. 5(b), showing in VFC estimation the "sharpening effect" of atmospheric correction (which results in a PAC image), that is, low estimation for low VFC and higher estimation for high VFC, but a "smoothing effect" of digital numbers, that is, higher estimation for low VFC and lower estimation for high VFC.

There are differences in acquirement conditions and processing methods of the images covering different areas, VI values of the same surface objects are then not coordinated on different images. Consequently, VI calibration is of great importance in VFC estimation using the VI-VFC models elsewhere (Cheng, 2006). Models established in this paper could not be directly applied to other places (time), unless the VI calibration is done through a calibration model (Zeng, 2004; Gu and Zeng, 2005). To establish the calibration model, three typical surface objects should be selected on both the image studied by us and images to study at other places (times). The three typical objects include clean deep water, dense vegetation, and dry bare land. VI values of each of these three typical objects are acquired respectively on the image studied by us and the images to study at other places (times), by averaging VI values (of often hundreds or thousands of

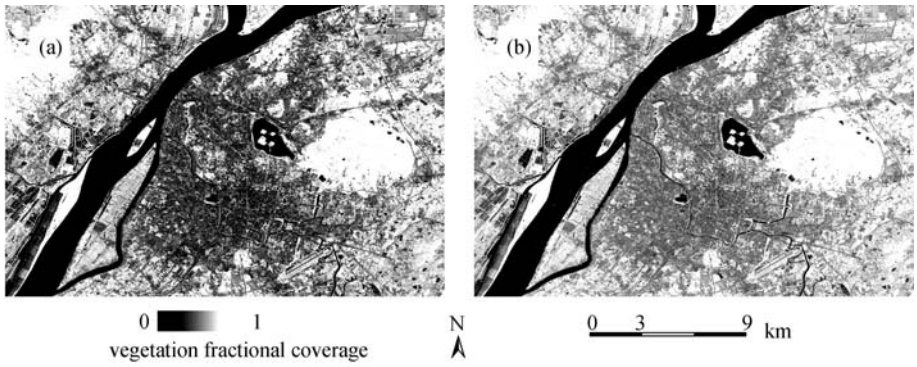

Fig. 5 Images of VFC calculation based on NDVI derived from PAC (a), and MSAVI derived from DN (b)

Table 3 VIs of clean deep water, dense vegetation and dry bare land of studied SPOT 5 images (mean±SD)

vegetation index	clean deep water	dense vegetation	dry bare land
NDVI[a]	0.10±0.02	0.71±0.03	0.38±0.01
TVI[a]	0.77±0.02	1.10±0.01	0.94±0.007
SAVI[b]	−0.52±0.01	0.23±0.06	−0.03±0.02
MSAVI[b]	−1.06±0.04	0.26±0.06	−0.04±0.03

Note: Each VI value was computed within about 300 to 1000 pixels.

pixels) for each of the corresponding objects. Then, three pairs of VI values are acquired, and the calibration model can be established from these three pairs of VI values via a least square algorithm. In other words, aided by four VIs derived from our SPOT 5 image in this study, together with the VIs acquired from the images to study at other places (times), a calibration model can be established, and then the four models shown in Table 2 can be used for VFC estimation from the images to study elsewhere (or at other times).

4 Conclusions

Given the different VFC ranges, VFC is positively related to the four VIs (i.e., NDVI, TVI, SAVI, and MSAVI), and the extension of the trend depends on vegetation types. Of all VFC estimating models using the four VIs as independent variables, the R^2 values of the models based on different radiometric correction levels ranked in terms of postatmospheric correction reflectance (PAC) > digital number (DN) > top of atmosphere reflectance (TOA). Under all radiometric correction levels, R^2 values of the models based on different polynomial models showed an order of linear ⩽quadratic⩽cubic, where the differences are dependent on vegetation indices and radiometric correction levels. Interactions exist in the impact of radiometric corrections, vegetation indices, and model types on the accuracy of VFC estimations. The degree of such interactions varies on different VFC ranges, which determines in a way the effect of radiometric corrections on the inversion of vegetation parameters (Qi et al., 2000; Liang et al., 2002; Liu et al., 2006b; Soudani et al., 2006). In quantitative remote sensing of vegetation parameters, the three key steps, that is, preprocessing of remote sensing image (e.g., radiometric corrections), parameterization of remote sensing information (e.g., vegetation indices), and the selection of inversion models (including empirical models and physical models) are important sources of uncertainties in estimation results and thus require further investigation. In VI-VFC modeling, taking these uncertain factors into consideration is helpful for mining remote sensing information and improving the accuracy of VFC estimation.

Acknowledgements This study was funded by the National Basic Research Program of China (No.2007CB407206) and the National Natural Science Foundation of China (No. 40371053). The authors thank Prof. Zhang Ganlin and Prof. Zhao Yuguo, Institute of Soil Science, Chinese Academy of Sciences, for technical helps with this study.

References

Abdou W A, Pilorz S H, Helmlinger M C, Conel J E, Diner D J, Bruegge C J, Martonchik J V, Gatebe C K, King M D, Hobbs P V (2000). Sua pansurface bidirectional reflectance: A case study to evaluate the effect of atmospheric correction on the surface products of the multi-angle imaging Spectro Radiometer (MISR) during SAFARI 2000. IEEE Trans Geosci Remote Rens, 44: 1699–1706

Cai T J, Ju C Y, Yao Y F (2005). Quantitative estimation of vegetation coverage in Mu Us sandy land based on RS and GIS. Chin J Appl Ecol, 16(12): 2301–2305 (in Chinese)

Carlson T N, Perry E M, Schmugge T J (1990). Remote estimation of soil moisture availability and fractional vegetation cover for agricultural fields. Agric For Meteorol, 52: 45–69

Chavez P S (1988). An improved dark-object subtraction technique for atmospheric scattering correction of multispectral data. Remote Sens Environ, 24: 459–479

Chen F, Zhou Z X, Wang P C,Li H F,Zhong Y F (2006). Green space vegetation quantity in workshop area of Wuhan Iron and Steel Company. Chin J Appl Ecol, 17(4): 59–596 (in Chinese)

Cheng Q (2006). Multi-sensor comparisons for validation of MODIS vegetation indices. Pedosphere, 16: 362–370

Dymond J R, Stephens P R, Newsome P F, Wilde R H (1992). Percent vegetation cover of a degrading rangeland from SPOT. Intl J Remote Sens, 13: 1999–2007

Eastwood J A, Yates M G, Thomson A G, Fuller R M (1997). The reliability of vegetation indices for monitoring saltmarsh vegetation cover. Intl J Remote Sens, 18: 3901–3907

Gao S H, , Guo J P, Liu L, Liu A L, Deng F D (2001). Study on remote sensing interpretation of vegetation coverage and calculation of water and soil conservation effect coefficient in northern region of China. J Soil Water Conserv, 15(3): 65–67 (in Chinese)

Gemmell F, Vajo J, Strandstrom M (2001). Estimating forest cover in a boreal forest test site using the mapper data from two dates. Remote Sens Environ, 77: 197–211

Gitelson A A, Kaufman Y J, Stark R, Rundquist D, Kaufman Y J (2002). Novel algorithms for remote estimation of vegetation fraction. Remote Sens Environ, 80: 76–87

Gong J Z, Xia B C (2006). Temporal-spatial characteristics and grading structure of vegetation fraction based on TM image in Guangzhou. J Plant Res Environ, 15(4): 25–29 (in Chinese)

Graetz R D, Pech R P, Davis A W (1988). The assessment and monitoring of sparsely vegetated rangelands using calibrated Landsat data. Int J Remote Sens, 9: 1201–1222

Gu Z J, Zeng Z Y(2005). Overview of researches on vegetation coverage in remote sensing. Res Soil Water Conserv, 12(2): 18–21 (in Chinese)

Hai C X, Liu B Y, Zhao Y (2002). Influence of soil humidity and vegetation coverage on wind erosion. Chin J Appl Ecol, 13(8): 1057–1058 (in Chinese)

He W Q, Zhao C X, Gao W S, Chen Y Q, Qin H L, Fan X R (2005). Main affecting factors of soil wind erosion under different land use patterns: A case study in Wuchuan County, Inner Mongolia. Chin J Appl Ecol, 16(11): 2092–2096 (in Chinese)

Huete A R, Jackson R D (1988). Soil and atmosphere influences on the spectra of partial canopies. Remote Sens Environ, 25: 89–105

Jiangsu Bureau of Surveying and Mapping (1997). Atlas of Jiangsu Province. Guangzhou: Guangdong Mapping Press (in Chinese)

Liang S L, Fang H L, Morisette J T, Chen M Z, Shuey C J, Walthall C L, Daughtry C S T (2002). Atmospheric correction of Landsat ETM^{+} land surface imagery. II. Validation and applications. IEEE Trans Geosci Remote Sens, 4: 2736–2746

Lin Z S, Qi X Z (2004). Vegetation evolution with degenerating soil ecology under unequal competition. Pedosphere, 14(3): 355–361

Liu D D, Ma J H, Yi D P (2006a). Vegetation cover influencing research of the atmosphere correction application on re-investigation of land use situation. J Heilongjiang Institute Tech, 20(2): 23–26 (in Chinese)

Liu Z Y, Huang J F, Wu X H,Dong Y P, Wang F M, Liu P T (2006b). Hyperspectral remote sensing estimation models on vegetation coverage of natural grassland. Chin J Appl Ecol, 17(6): 997–1002 (in Chinese)

McDaniel K C, Haas R H (1982). Assessing mesquite-grass vegetation condition from Landsat. Photo Eng Remote Sens, 48: 441–450

North P R J (2002). Estimation of APAR, LAI, and vegetation fractional cover from ATSR imagery. Remote Sen Environ, 80: 114–121

Purevdorj T, Tateishi R, Ishiyama T, Honda Y (1998). Relationship between percent vegetation cover and vegetation indices. Intl J Remote Sens, 19: 3519–3535

Qi J, Chehbouni A, Huete A R, Kerr Y H, Sorooshian S (1994). A modified soil adjusted vegetation index (MSAVI). Remote Sens Environ, 48: 119–126

Qi J, Marsett R C, Moranb M S, Goodrich D C, Heilman P, Kerr Y H, Dedieu G, Chehbouni A, Zhang X X (2000). Spatial and temporal dynamics of vegetation in the San Pedro River basin area. Agric For Meteorol, 105: 55– 68

Ringrose S, Matheson W, Wolski P, Huntsman-Mapila P (2003). Vegetation cover trends along the Botswana Kalahari transect. J Arid Environ, 54: 297–317

Rouse J W, Haas R H, Schell J A, Deering D W (1973). Monitoring vegetation systems in the great plains with Erts Freden SC, ed. Third Earth Resources Technology Satellite-1 Symposium. Volume I: Technical Presentations. Washington, DC: NASA, 309–317

Song C, Woodcock C E, Seto K C, Lenney M P, Macomber S A (2001). Classification and change detection using Landsat TM data: When and how to correct atmospheric effects? Remote Sens Environ, 75: 230–244

Soudani K, Francois C, leMaire G, Le Dantec V, Dufrêne E (2006). Comparative analysis of IKONOS, SPOT, and ETM^{+} data for leaf area index estimation in temperate coniferous and deciduous forest stands. Remote Sens Environ, 102: 161–175

Sun R, Liu C M, Zhu Q J (2001). Relationship between the fractional vegetation cover change and rainfall in the Yellow River Basin. Acta Geo Sinica, 56(6): 667–672 (in Chinese)

Wittich K P, Hansing O (1995). Area-averaged vegetative cover fraction estimated from satellite data. Int J Biomete-orol, 38: 209–215

Yu Q, Gong P, Clinton N, Biging G, Kelly M, Schirokauer D (2006). Object-based detailed vegetation classification with airborne high spatial resolution remote sensing imagery. Photo Eng Remote Sens, 72: 799–811

Zeng Z Y (2004). Research on Computer Classification of Satellite Images and Application in Geo-science. Beijing: Science Press (in Chinese)

Zhang W B, Liu B Y, Wu J D (2001). Monitoring of plant coverage of plots by visual estimation and overhead photograph. Bull Soil Water Conserv, 21(6): 60–63 (in Chinese)

Zhang Y X, Zhang Y F, Li X B (2007). The synthetically estimating vegetation fractional coverage of grassland using field data and A STER remote sensing imagine. Acta Ecol Sinica, 27(3): 964–976 (in Chinese)

Zhao H L, Zhang T H, Zhao X Y, Zhou R L (2004). Effect of grazing on sandy grassland ecosystem in Inner Mongolia. Chin J Appl Ecol, 15 (3): 420–424 (in Chinese)